J Eng Math (2007) 59:1–23
DOI 10.1007/s10665-006-9117-3

ORIGINAL PAPER

Thermal-stress reduction for a Czochralski grown single crystal

Huaxiong Huang · Shuqing Liang

Received: 8 September 2005 / Accepted: 13 September 2006 / Published online: 1 December 2006

Abstract In this paper an optimal-control approach for thermal-stress reduction inside a Czochralski-grown single crystal is presented. Using the lateral heat flux as a control variable, an optimal-control formulation for minimizing thermal stress with a given crystal shape is derived. Since the thermal stress is also affected by the lateral shape of crystals during growth, the level of the stress can be reduced by growing crystals into a suitable shape. Using the lateral shape as a control variable, a similar optimal-control formulation for stress reduction is derived. In both cases, the von Mises stress is used as an objective function for the constrained optimization problem. Euler–Lagrange equations are derived using the calculus of variations and Lagrange multipliers. Various stress-reduction strategies are explored by solving the Euler–Lagrange equations numerically.

Keywords Calculus of variations · Crystal · Czochralski technique · Optimal control · von Mises stress

1 Introduction

The Czochralski (Cz) technique is one of the most common methods for growing single semiconductor crystals. The quality of Cz-grown crystals is affected greatly by crystalline defects formed during the growth process. It is well-known that defect density is directly related to the thermal stress caused by temperature variation inside the crystal [1, 2]. Therefore, it is important to find a systematical way to control the temperature variation during growth.

Several researchers have utilized optimal-control approaches to find favorable growth conditions with properly chosen objective functions for growing cylindrical silicon crystals with constant radii. For example,

H. Huang
School of Mathematics
Fudan University
Shanghai, 200433, China

H. Huang · S. Liang (✉)
Department of Mathematics and Statistics, York University, Toronto, Ontario, Canada M3J 1P3
e-mail: sqliang@yorku.ca

H. Huang
e-mail: hhuang@yorku.ca

Bornside et al. [1] used the von Mises stress as a measure of thermal stress to find optimum growth conditions and system configurations for dislocation-free Cz-grown silicon crystals. They applied an integrated numerical-analysis model to search for optimal growth conditions. Using a carefully selected target temperature distribution, Müller [3] showed that the optimum growth conditions for the silicon Czochralski process can be found by optimizing the geometry of hot-zone heat shields and cooling devices. Jeong and Kang [4] obtained optimal conditions by using the crystal-surface temperature distribution as an objective function. All of the above studies assume cylindrical crystals and none has discussed the effect of crystal lateral shape on the thermal-stress distribution.

By comparison, much less attention has been paid to compound crystal growth where controlling the appearance of crystalline defects is more difficult. Care must be taken to control the lateral shape of the crystal, as well as the thermal environment. It has been shown that the lateral shape needs to be controlled carefully to avoid the appearance of excessive defects [5, 6]. This is mainly due to their low resistance to resolved shear stress which is responsible for causing crystalline defects [6, 7]. In practice, "magic shapes" are obtained by trial-and-error, based on the experience of the grower [7]. The main objective of this paper is to investigate stress-reduction strategies using a more systematical approach. We will set up an optimal-control approach which searches for favorable conditions automatically, by exploring the inter-play between thermal environment (lateral heat flux) and crystal shape.

Following [5], we derive an explicit formula for the von Mises stress and use it as a primary measure to set up a constrained-optimization problem within the framework of optimal control. In the first approach, we use the lateral heat flux as a control variable while the shape of the crystal is fixed, normally a cone. In the second approach, the crystal radius is used as a control variable while the lateral heat flux is assumed to be given. This two-step approach is not a mathematical necessity since a combined approach with two control variables (heat flux and radius) can be attempted and the mathematical setup is almost identical. It is adopted from a practical point of view since a complete control of the lateral heat flux may not be achievable. A more common strategy is to partially control the lateral heat flux, e.g. by using a heat shields, while adjusting the withdrawal rate and heater-power supply so that the crystal grows into a desirable shape.

While a full numerical approach using stress as a objective function [1] provides an accurate control over the stress level, it is normally computationally intensive due to the iterative nature of search algorithms during minimization. Furthermore, the results tend to be problem-specific, which may not be readily applicable to other growth processes with different setups. Using temperature as a control target is computationally more efficient as demonstrated in [3, 4, 8–10]. However, the control of the thermal stress is not directly imposed unless a priori knowledge of the growth process is available. In general, the relationship between temperature and stress is not readily available for a complex growth process such as Cz growth.

In this paper, we use an alternative approach by utilizing mathematical models to predict the temperature–stress relationship, under proper simplifications. In [5], a semi-analytical thermal-stress model is obtained using a perturbation approach with the Biot number (the non-dimensional heat flux through the lateral crystal surface) as a small parameter, similar to previous work [11–15]. In this study, we extend the model in [5] to allow for a variable heat flux between the lateral crystal surface and the ambient gas in the growth chamber. In principle, the lateral heat flux to the ambient gas can only be determined by solving the coupled heat-transfer problem involving the crystal, melt, gas, the configuration and heat supply of the grower. However, it can be altered or controlled using devices such as heat shields [3]. Therefore, it is reasonable to treat the lateral heat flux as a control variable in the optimization process. The shape of a Cz-grown crystal is determined by the motion of the triple-phase point, which can be controlled by the heater power supply and extracting rate. We can use it as another control variable. In practice, the dynamics of the triple point may be important due to stability of its radial motion [16, Chapter 2] . However, this effect can be minimized by using a feedback control device [8].

To keep our problem manageable, we have decoupled the melt as in [5]. We assume that the heat flux from the melt is uniform in the radial direction, based on the observation that the crystal–melt interface is almost flat for Cz-grown InSb crystals [7]. In reality, the heat flux at the interface is influenced by the melt

flow inside the crucible and is controlled indirectly by the heater. Additional control may be realized by using electromagnetic fields to alter the melt-flow pattern and its stability [17].

The rest of the paper is organized as follows. In Sect. 2, we present a semi-analytical model for the (von Mises) thermal stress and the setup of the optimal-control problems. In Sect. 3, we introduce a variational formulation and the Euler–Lagrange equations are derived using the calculus of variations, Lagrange multipliers and penalty functions. Numerical results and discussions are presented in Sect. 4 and we conclude with a short discussion in Sect. 5.

2 Problem description

The problem setup and the derivations of the asymptotic solutions for temperature and thermal stress are similar to those in [5]. For completeness, however, we will briefly describe the model and present the temperature and stress solutions before setting up our optimal-control problems. For a detailed description of the model and perturbation solution of the temperature, we refer the interested reader to [5] and references therein.

2.1 A semi-analytical model

Following [5], we assume that the crystal is axis-symmetric and the coordinate system is fixed to the top of the growing crystal at $z = 0$, the final length of the crystal is denoted by L and the crystal radius is denoted by $R(z)$. The growth starts with a seed crystal with a radius of order $R_0 = 5 \times 10^{-3}$ m and length $Z_0 = 3 \times 10^{-2}$ m. Figure 1 illustrates the geometry of a typical crystal. Within the crystal Ω, the temperature $T(\mathbf{x}, t)$ satisfies the heat equation

$$\rho_s c_s \frac{\partial T}{\partial t} = k_s \nabla^2 T, \quad \mathbf{x} \in \Omega,\ t > 0, \tag{1}$$

where ρ_s, c_s and k_s are the density, specific heat and thermal conductivity of the crystal (solid phase), respectively. The lateral surface of the crystal is denoted by Γ_g. The temperature boundary condition at the lateral surface is given as

$$-k_s \frac{\partial T}{\partial \mathbf{n}} = h_{gs}(T - T_g) + r_c(T^4 - T_g^4), \quad \mathbf{x} \in \Gamma_g. \tag{2}$$

where h_{gs} and r_c are the heat-transfer coefficients at the lateral surface due to convective cooling by the gas and radiative heat loss, respectively and T_g is the ambient gas temperature. Alternatively, we can model both convective and radiative effects through a simple Newtonian cooling law:

$$-k_s \frac{\partial T}{\partial \mathbf{n}} = h_{gs}(T - T_g), \quad \mathbf{x} \in \Gamma_g. \tag{3}$$

Here we assume that the heat-transfer coefficient, h_{gs}, incorporates both convective and radiative heat transfer (via linearization). At the top of the crystal we invoke a Newtonian cooling law

$$k_s \frac{\partial T}{\partial z} = h_{ch}(T - T_{ch}), \quad z = 0, \tag{4}$$

in the case that the radius at $z = 0$ is assumed to be non-zero. Here h_{ch} represents the heat-transfer coefficient for the seed-chuck connection and T_{ch} is the chuck temperature.

The crystal–melt interface is denoted by Γ_S where $T = T_m$ (melting temperature). The solidus isotherm is thus implicitly defined by the temperature field. Explicitly, we denote the solidus isotherm by

$$z - S(\mathbf{x}, t) = 0, \quad \mathbf{x} \in \Gamma_S. \tag{5}$$

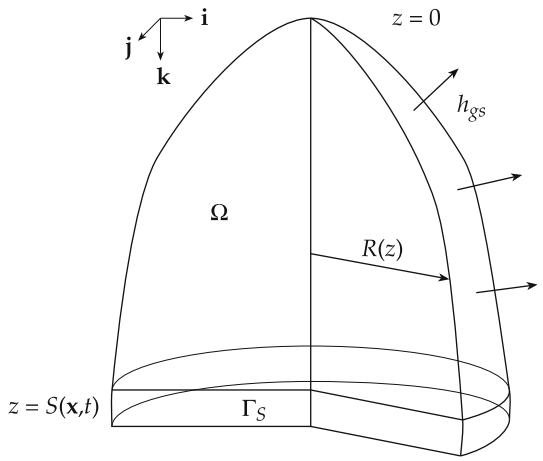

Fig. 1 A typical crystal at some time t during a growth run with a newly solidified portion at $z = S(\mathbf{x}, t)$ [5]

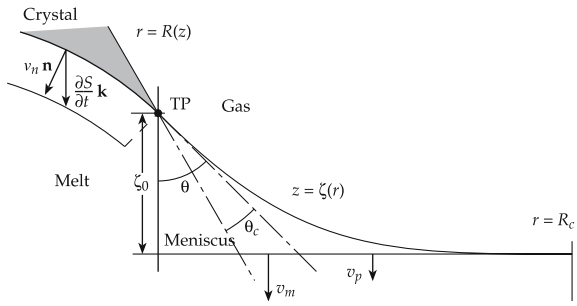

Fig. 2 Schematic diagram of the meniscus $z = \zeta(r)$ with capillary height ζ_0 [5]

The motion of the solidus isotherm is governed by the Stefan condition

$$\rho_s L_h \left|\vec{v}_n\right| = k_s \frac{\partial T}{\partial \mathbf{n}}\bigg|_{z\to S^-} - q_{l,n}, \tag{6}$$

where $|\vec{v}_n|$ is the speed at which the interface moves in the direction of the outward unit normal $\mathbf{n}$, L_h is the latent heat and $q_{l,n}$ is the heat flux from the melt normal to the interface.

The crystal radius is determined by the motion of the melt–solid–gas triple point, which is given by

$$\frac{\partial R}{\partial t}\bigg|_{z=S} = \tan(\theta - \theta_c)\frac{\partial S}{\partial t}\bigg|_{r=R}, \tag{7}$$

where θ_c is the contact angle formed by the wetting fluid (melt) and the crystal and θ is the angle formed by the meniscus with the vertical z-axis.

For the size of the crystals under consideration here, the effect of the surface tension in the azimuthal direction can be neglected. Furthermore, if we disregard the dynamic effect of the melt flow, the shape of the meniscus is determined by the surface tension through the Laplace–Young equation and the capillary height ζ_0 at the triple junction is approximately [18]

$$\zeta_0 = \sqrt{\alpha\,(1 - \sin\theta)}, \tag{8}$$

where $\alpha = 2\sigma/\rho_l g$, σ the surface-tension coefficient, ρ_l the density of melt, and g the gravitational constant. Figure 2 shows the schematic diagram of the meniscus. From mass conservation, the change of the capillary height ζ_0 at the triple junction is defined by

$$\frac{\mathrm{d}\zeta_0}{\mathrm{d}t} = v_p + v_m - \frac{\partial S}{\partial t}, \tag{9}$$

where v_p is the pulling rate and v_m is the rate at which the melt/gas surface drops, which is given by

$$v_m = \frac{\rho_s R^2}{\rho_l R_c^2}\frac{\partial S}{\partial t},$$

where R_c is the radius of the crucible. Thus, the meniscus shape is determined by its height, which is controlled by the heat fluxes and crystal-extraction (pulling) rate.

2.1.1 Asymptotic solution

Define the Biot number by

$$\epsilon = \frac{\bar{h}_{gs}\overline{R}}{k_s},$$

where $\bar{h}_{gs}$ is the mean heat-transfer coefficient defined by

$$\bar{h}_{gs} = \frac{1}{L}\int_0^L h_{gs}(z)\,\mathrm{d}z,$$

where L is the final length of the crystal.

In the same spirit as in [5], we now non-dimensionalize the equation and boundary conditions using the following scalings

$$r = \overline{R}\hat{r}, \quad \epsilon^{1/2}z = \overline{R}\hat{z}, \quad R(z) = \overline{R}\hat{R}(\hat{z}), \quad \epsilon^{1/2}S(r,t) = \overline{R}\hat{S}(\hat{r},\hat{t}),$$

$$T = T_g + \Delta T\Theta, \quad \Delta T = T_m - T_g, \quad t = \frac{\mathrm{S_T}\overline{R}^2\rho_s c_s}{k_s\epsilon}\hat{t}, \quad \mathrm{S_T} = \frac{L_h}{c_s\Delta T}.$$

Here variables with hats ($\hat{}$) are non-dimensional. In the following, the hats will be dropped for brevity. The non-dimensional equation and boundary conditions are

$$\frac{\epsilon}{\mathrm{S_T}}\Theta_t = \frac{1}{r}(r\Theta_r)_r + \epsilon\Theta_{zz}, \quad \mathbf{x}\in\Omega,\ t>0, \tag{10}$$

$$\begin{aligned} &-\Theta_r + \epsilon\Theta_z R'(z) = \epsilon\left[1+\epsilon(R'(z))^2\right]^{1/2}(\beta\Theta + f(\Theta)), && \mathbf{x}\in\Gamma_g,\\ &\Theta = 1, && \mathbf{x}\in\Gamma_S,\\ &\Theta_z = \delta_0(\Theta-\Theta_{ch}), && z=0, \end{aligned} \tag{11}$$

where $\beta(z) = h_{gs}(z)/\bar{h}_{gs}, f(\Theta) = r_c/\bar{h}_{gs}\left(\Delta T^3\Theta^4 + 4T_g\Delta T^2\Theta^3 + 6T_g^2\Delta T\Theta^2 + 4T_g^3\Theta\right)$ and $\delta_0 = \epsilon^{1/2}h_{ch}/\bar{h}_{gs}$.

The solidus advances according to the Stefan condition (6) which, in non-dimensional coordinates, becomes

$$\Theta_z - \frac{1}{\epsilon}S_r\Theta_r = (\gamma + S_t), \quad \gamma = \frac{q_l\overline{R}}{\epsilon^{1/2}k_s\Delta T}, \tag{12}$$

where q_l and γ are the dimensional and dimensionless heat fluxes in the liquid across the crystal/melt interface in the axial direction. As discussed in [5], we assume that the solidification is driven by the heat loss from the lateral crystal surface and the rate of solidification defines the relevant time scale. Equation 12 simply states that the motion of the interface is determined by the heat conduction in the solid as well as in the melt. After the rescaling, the heat conduction in the crystal is an order-one quantity. Therefore, the rescaled heat flux from the melt γ must be of order one at most.

To find an asymptotic solution for the temperature, we expand both Θ and S in terms of ϵ as in [5]. Equations 10 and 11 suggest that the temperature Θ is independent of r to leading order. Consequently, the crystal/melt interface S is also independent of r to leading order. Based on these observations, we expand both Θ and S as follows:

$$\begin{aligned} &\Theta \sim \Theta_0(z,t) + \epsilon\Theta_1(r,z,t) + \epsilon^2\Theta_2(r,z,t) + \cdots,\\ &S \sim S_0(t) + \epsilon S_1(r,t) + \epsilon^2 S_2(r,t) + \cdots. \end{aligned} \tag{13}$$

If we substitute the expansion in the scaled model (10) and (11), collect the terms at the zeroth and first order of ϵ, and apply the solvability conditions, we can derive the equations for the leading- and higher-order solutions. The detailed derivations can be found in [5, 19]. A similar and more detailed asymptotic analysis for cylindrical crystals can be found in [11, 12, 15].

The zeroth-order temperature solution satisfies

$$\frac{1}{S_T}\Theta_{0,t} = \Theta_{0,zz} + \frac{2}{R}\left[R'\Theta_{0,z} - \beta\Theta_0 - f(\Theta_0)\right], \quad 0 < z < S_0(t),\ t > 0, \tag{14a}$$

$$\Theta_{0,z} = \delta_0(\Theta_0 - \Theta_{ch}), \quad z = 0, \tag{14b}$$

$$\Theta_0 = 1, \quad z = S_0(t) \tag{14c}$$

with an initial condition $\Theta_0(z,0) = g(z) \leq 1$ compatible with the boundary conditions.

The advance of $S_0(t)$ is coupled to the thermal gradients via

$$\gamma + S_{0,t} = \Theta_{0,z}\big|_{z=S_0(t)}, \tag{15}$$

where $S_0(0) = Z_0$.

Since there is a one-to-one relationship between growth time t and the size of the crystal (given by S_0), we use S_0 as the main variable, instead of t. In addition, as the lateral size of the crystal is determined by the motion of the triple junction, which can be controlled by the pulling rate and thermal flux from the melt, we will work with the crystal radius directly. In some of the computations reported in this study, we have used the non-dimensional version of Eq. 7 for the radial motion of the triple junction where the value of θ is given by (8).

2.1.2 Thermal stress

Based on the plane-strain assumption, the thermal stress can be obtained as

$$\sigma_{rr} = \frac{1}{4}\overline{\sigma}\left(R(z)^2 - r^2\right), \quad \sigma_{\theta\theta} = \frac{1}{4}\overline{\sigma}\left(R(z)^2 - 3r^2\right), \quad \sigma_{zz} = \frac{1}{2}\overline{\sigma}\left(R(z)^2 - 2r^2\right), \tag{16}$$

where $\overline{\sigma} = \epsilon\Theta_1^1(z,t)$, $\Theta_1^1(z,t) = \frac{1}{2R(z)}[R'(z)\Theta_{0,z}(z,t) - \beta(z)\Theta_0(z,t) - f(\Theta_0(z,t))]$. The von Mises stress is

$$\begin{aligned}\sigma_{\text{VM}} &= \frac{1}{\sqrt{2}}\left[(\sigma_{rr} - \sigma_{\theta\theta})^2 + (\sigma_{rr} - \sigma_{zz})^2 + (\sigma_{\theta\theta} - \sigma_{zz})^2\right]^{1/2} \\ &= \frac{1}{4}\epsilon\left|\Theta_1^1(z,t)\right| R(z)^2\left[1 - 4\left(\frac{r}{R(z)}\right)^2 + 7\left(\frac{r}{R(z)}\right)^4\right]^{1/2}.\end{aligned} \tag{17}$$

In the pseudo-steady case $\Theta_{0,zz} = -4\Theta_1^1$, so that Eq. 17 becomes

$$\begin{aligned}\sigma_{\text{VM}} &= \frac{1}{16}\epsilon\left|\Theta_{0,zz}(z)\right| R(z)^2\left[1 - 4\left(\frac{r}{R(z)}\right)^2 + 7\left(\frac{r}{R(z)}\right)^4\right]^{1/2} \\ &= \frac{1}{8}\epsilon\left|\left(R'(z)\Theta_{0,z}(z) - \beta(z)\Theta_0(z) - f(\Theta_0)\right)\right| R(z) \\ &\quad \times\left[1 - 4\left(\frac{r}{R(z)}\right)^2 + 7\left(\frac{r}{R(z)}\right)^4\right]^{1/2}.\end{aligned} \tag{18}$$

Remark If we use (3) as the temperature boundary condition, we can obtain an asymptotic solution and thermal stress by setting $f(\Theta_0) = 0$ in the above equations.

2.2 Stress minimization

We now discuss the main objective of this paper. We will use the analytical formula for the von Mises stress (18) and set up our optimization problems. Since the von Mises stress depends on the heat-transfer coefficient h_{gs} (or more precisely $\beta(z)$), as well as crystal shape $R(z)$, we will discuss two problems. In the first approach we use $\beta(z)$ as a control variable, while keeping the crystal shape $R(z)$ fixed. In the second problem we use $R(z)$ as a control variable with $\beta(z)$ fixed.

2.2.1 Problem I: Optimal $\beta(z)$

The original mathematical statement of the problem at hand is

$$\min_{\beta(z)} \max_{Z_0 \le S_0 \le L, 0 \le z \le S_0, 0 \le r \le R(z)} \sigma_{\text{VM}}(r, z; R, S_0, \beta)$$

subject to constraints, where Z_0 and L are the length of the seed and the final length of the crystal, respectively. However, this set-up is not easy to handle numerically. We seek an approximation for this problem as follows

$$\min_{\beta(z)} \left[\int_0^L \sigma_{\text{VM}}^2(z) \mathrm{d}z + \omega_1 \int_0^L (\beta(z) - \beta_0)^2 \, dz - \omega_2 \int_0^L \Theta_{0,z}^2(z) \mathrm{d}z \right]$$

subject to

$$\Theta_{0,zz} + \frac{2}{R}\left[R'\Theta_{0,z} - \beta\Theta_0 - f(\Theta_0)\right] = 0, \quad 0 < z < L, \tag{19a}$$

$$\Theta_{0,z} = \delta_0(\Theta_0 - \Theta_{ch}), \quad z = 0, \tag{19b}$$

$$\Theta_0 = 1, \quad z = L, \tag{19c}$$

$$\int_0^L \beta(z) \mathrm{d}z = \beta_0 L, \tag{19d}$$

$$\beta(z) \ge 0, \quad 0 \le z \le L, \tag{19e}$$

where $0 \le \omega_k \le 1$ are weighting parameters and β_0 is a given parameter. The first term of the objective functional is the L^2 version of the original functional. The second term is a penalty term added to avoid drastic variation in β, which could be impractical to implement. The last term is also a term that penalizes slow growth, which may also be undesirable from a practical point of view. The integral constraint on β is for comparison purposes since stress reduction due to a smaller mean heat flux should be considered a real benefit. Obviously, the heat-transfer coefficient must remain positive from a physical point of view. Here we have used the pseudo-steady approximation. In this case the von Mises stress becomes

$$\sigma_{\text{VM}} = \frac{1}{8}\epsilon \left|R'(z)\Theta_{0,z}(z) - \beta(z)\Theta_0(z) - f(\Theta_0)\right| R(z) \left[1 - 4\left(\frac{r}{R(z)}\right)^2 + 7\left(\frac{r}{R(z)}\right)^4\right]^{1/2}$$

which reaches its maximum when $r = R$, i.e.,

$$\sigma_{\text{VM}} \le \frac{1}{4}\epsilon \left|R'(z)\Theta_{0,z}(z) - \beta(z)\Theta_0(z) - f(\Theta_0)\right| R(z).$$

Thus, our optimization problem can be changed into

$$\min_{\beta(z)} \left[\int_0^L \left[\left(R'(z)\Theta_{0,z}(z) - \beta(z)\Theta_0(z) - f(\Theta_0)\right) R(z)\right]^2 \mathrm{d}z + \omega_1 \int_0^L (\beta(z) - \beta_0)^2 \, \mathrm{d}z - \omega_2 \int_0^L \Theta_{0,z}^2(z) \mathrm{d}z \right] \tag{20}$$

with the constraints.

2.2.2 Problem II: shape optimization

Similarly we seek an approximation and set up the problem as follows

$$\min_{R(z)} \left[\int_0^L \sigma_{\text{VM}}^2(z) \mathrm{d}z + \omega_1 \int_0^L \left(R'(z) - R_0'\right)^2 \mathrm{d}z - \omega_2 \int_0^L \Theta_{0,z}^2(z) \mathrm{d}z \right],$$

or

$$\min_{R(z)} \left[\int_0^L \left[\left(R'(z)\Theta_{0,z}(z) - \beta(z)\Theta_0(z) - f(\Theta_0(z)) \right) R(z) \right]^2 \mathrm{d}z \right.$$
$$\left. + \omega_1 \int_0^L \left(R'(z) - R'_0 \right)^2 \mathrm{d}z - \omega_2 \int_0^L \Theta_{0,z}^2(z)\mathrm{d}z \right], \tag{21}$$

subject to

$$R\Theta_{0,zz} + 2\left(R'\Theta_{0,z} - \beta\Theta_0 - f(\Theta_0) \right) = 0, \quad 0 < z < L, \tag{22a}$$
$$\Theta_{0,z} = \delta_0(\Theta_0 - \Theta_{ch}), \quad z = 0, \tag{22b}$$
$$\Theta_0 = 1, \quad z = L, \tag{22c}$$
$$\int_0^L R^2(z)\mathrm{d}z = L, \tag{22d}$$
$$R = R_0, \quad z = 0, \tag{22e}$$
$$R(z) \geq R_0, \quad 0 \leq z \leq L, \tag{22f}$$

where R_0 and R'_0 are given parameters and ω_k are penalty parameters. The first and last term in the objective functional are the same as before. The second term is added to penalize deviation from a conical shape. From a practical point of view, drastic variation of the crystal shape should be avoided, since it may reduce the usable amount of the material. In addition, there exists a critical growth angle for some compound crystals beyond which twinning may happen during growth [20].

3 Derivation of the Euler–Lagrange equations

We now discuss the Euler–Lagrange equations for the two optimization problems using the calculus of variations.

3.1 Problem I

Since the constraints include the two equality constraints (19a), (19d) and inequality (19e), we use the method of Lagrange multipliers and the penalty-function method. The augmented Lagrangian objective function is defined by

$$J_1 = \int_0^L \left[\left(R'(z)\Theta_{0,z}(z) - \beta(z)\Theta_0(z) - f(\Theta_0(z)) \right) R(z) \right]^2 \mathrm{d}z$$
$$+ \int_0^L \lambda(z) \left[\Theta_{0,zz}(z) + \frac{2}{R(z)} \left(R'(z)\Theta_{0,z}(z) - \beta(z)\Theta_0(z) - f(\Theta_0(z)) \right) \right] \mathrm{d}z$$
$$+ \omega_1 \int_0^L \left(\beta(z) - \beta_0 \right)^2 \mathrm{d}z - \omega_2 \int_0^L \Theta_{0,z}^2(z)\mathrm{d}z$$
$$+ \mu \left(\beta_0 L - \int_0^L \beta(z)\mathrm{d}z \right) + \frac{\rho}{2} \int_0^L \beta^2(z) H(-\beta(z))\mathrm{d}z, \tag{23}$$

where $\lambda(z)$ and μ are Lagrange multipliers, ρ is a penalty parameter which is a sufficiently large positive number, and $H(\cdot)$ is the Heaviside function.

Using the calculus of variations, we can derive the necessary conditions based on first-order variations. For the optimization problem given by (23) with constraints (19a–19e), we obtain the following

Euler–Lagrange equations (see Appendix A for a detailed derivation)

$$\Theta_{0,zz} + \frac{2}{R}\left[R'\Theta_{0,z} - \beta\Theta_0 - f(\Theta_0)\right] = 0, \tag{24a}$$

$$\int_0^L \beta(z)\mathrm{d}z = \beta_0 L, \tag{24b}$$

$$2R^2\left(R'\Theta_{0,z} - \beta\Theta_0\right)\Theta_0 + 2\lambda\Theta_0/R - 2\omega_1\left(\beta - \beta_0\right) + \mu - \rho\beta H(-\beta) = 0, \tag{24c}$$

$$\begin{aligned}&\lambda_{zz} - \left(\frac{2R'\lambda}{R}\right)_z - 2\lambda\beta/R - 2\beta R^2\left(R'\Theta_{0,z} - \beta\Theta_0\right)\\ &\quad - 2\left(R^2R'\left(R'\Theta_{0,z} - \beta\Theta_0\right)\right)_z - 2R^2\left(R'\Theta_{0,z} - \beta\Theta_0 - f(\Theta_0)\right)f'(\Theta_0)\\ &\quad + 2R^2\beta f(\Theta_0) - 2\left(2RR'^2 f(\Theta_0) + R^2R''f(\Theta_0) + R^2R'f'(\Theta_0)\Theta_{0,z}\right)\\ &\quad - 2\lambda f'(\Theta_0)/R + 2\omega_2\Theta_{0,zz} = 0.\end{aligned} \tag{24d}$$

The boundary conditions for the above equations are

$$\Theta_{0,z} = \delta_0(\Theta_0 - \Theta_{ch}), \quad z = 0, \tag{25a}$$

$$\Theta_0 = 1, \quad z = L, \tag{25b}$$

$$\lambda_z - \left(\delta_0 + \frac{2R'}{R}\right)\lambda - 2R^2R'\left[\left(R'\delta_0 - \beta\right)\Theta_0 - R'\delta_0\Theta_{ch}\right] - 2R^2R'f(\Theta_0) = 0, \quad z = 0, \tag{25c}$$

$$\lambda = 0, \quad z = L. \tag{25d}$$

This is a system of coupled nonlinear second-order ordinary differential equations for the temperature Θ and a Lagrange multiplier λ. In general, it has to be solved numerically.

3.2 Problem II

Similarly we use Lagrange multipliers to derive the Euler–Lagrange equations. The augmented Lagrangian objective function is defined by

$$\begin{aligned}J_2 = &\int_0^L \left[\left(R'(z)\Theta_{0,z}(z) - \beta(z)\Theta_0(z) - f(\Theta_0(z))\right)R(z)\right]^2\mathrm{d}z\\ &+\omega_1\int_0^L \left(R'(z) - R_0'\right)^2\mathrm{d}z - \omega_2\int_0^L \Theta_{0,z}^2(z)\mathrm{d}z\\ &+\int_0^L \lambda(z)\left[R(z)\Theta_{0,zz}(z) + 2\left(R'(z)\Theta_{0,z}(z) - \beta(z)\Theta_0(z) - f(\Theta_0(z))\right)\right]\mathrm{d}z\\ &+\mu\left[L - \int_0^L R^2(z)\mathrm{d}z\right] + \frac{\rho}{2}\int_0^L \left(R(z) - R_0\right)^2 H(R_0 - R(z))\mathrm{d}z\end{aligned} \tag{26}$$

where $\lambda(z)$ and μ are Lagrange multipliers, $\rho > 0$ is a penalty parameter and $H(\cdot)$ is the Heaviside function.

Using the calculus of variation, we can derive necessary conditions for the optimization problem given by (26) with the constraints (22a–22f). We obtain the following Euler–Lagrange equations (details in Appendix B)

$$R\Theta_{0,zz} + 2\left(R'\Theta_{0,z} - \beta\Theta_0 - f(\Theta_0)\right) = 0 \tag{27a}$$

$$\int_0^L R^2(z)\mathrm{d}z = L \tag{27b}$$

$$6RR'^2\Theta_{0,z}^2 - 12\beta\Theta_0 RR'\Theta_{0,z} + 6\beta^2 R\Theta_0^2 - 2R^2R''\Theta_{0,z}^2 + 2\beta' R^2\Theta_0\Theta_{0,z} - 2\omega_1 R''$$
$$+ 2\beta R^2\Theta_{0,z}^2 - \lambda\Theta_{0,zz} - 2\lambda'\Theta_{0,z} - 2\mu R + \rho\,(R - R_0)\,H(R_0 - R)$$
$$- 4RR'\Theta_{0,z}f(\Theta_0) + 6R^2f^2(\Theta_0) + 8R\beta\Theta_0 f(\Theta_0) + 2R^2f'(\Theta_0)\Theta_{0,z}^2 = 0 \tag{27c}$$

$$2\beta^2R^2\Theta_0 + 2R\left(\beta R\Theta_0 - 2RR'\Theta_{0,z}\right)R'' + 2\beta' R^2R'\Theta_{0,z} + R\lambda'' - \lambda R'' - 2\beta\lambda$$
$$+ 2R^2\beta\Theta_0 f'(\Theta_0) + 2R^2f(\Theta_0)f'(\Theta_0) + 4RR'2f(\Theta_0) + 2R^2R''f(\Theta_0)$$
$$+ 2R^2\beta f(\Theta_0) - 2\lambda f'(\Theta_0) + 2\omega_2\Theta_{0,zz} = 0. \tag{27d}$$

The boundary conditions are

$$\Theta_{0,z} = \delta_0(\Theta_0 - \Theta_{ch}), \quad z = 0, \tag{28a}$$

$$\Theta_0 = 1, \quad z = L, \tag{28b}$$

$$\left(\frac{\lambda}{R}\right)' + 2R'\left[\beta\Theta_0 - \delta_0 R'\,(\Theta_0 - \Theta_{ch})\right] + 2\omega\delta_0\,(\Theta_0 - \Theta_{ch})$$
$$+ 2R^2R'f(\Theta_0) = 0, \quad z = 0, \tag{28c}$$

$$\lambda = 0, \quad z = L, \tag{28d}$$

$$R = R_0, \quad z = 0, \tag{28e}$$

$$2R^2\left(R_z\Theta_{0,z} - \beta\right)\Theta_{0,z} + 2\lambda\Theta_{0,z} + 2\omega_1\left(R' - R_0'\right) - R^2f(\Theta_0)\Theta_{0,z} = 0, \quad z = L. \tag{28f}$$

3.3 Numerical implementation

The system of equations (24a–24d) with boundary conditions (25a–25d) and Eqs. 27a–27d with boundary conditions (28a–28f) are nonlinear and coupled. In order to solve them, we use a finite-difference method to discretize the differential equations and use a trapezoidal rule for the integrals. The discrete system is also a nonlinear system and is solved using MATLAB. MATLAB uses a Gauss–Newton method and a trust-region dogleg method to solve the nonlinear systems of equations. The Gauss–Newton method uses a nonlinear least-squares solver which employs a line-search procedure and a quasi-Newton method to solve the equations. Newton's method is used in a trust-region dogleg method to find the search direction.

4 Results

Two sets of computations are carried out, one corresponding to temperature boundary condition (3) and the other with temperature boundary condition (2). Using the optimality system of Eqs. 24a–24d with boundary conditions (25a–25d), we can find the optimal heat-transfer coefficient h_{gs} for given crystal shapes. The optimal crystal shape is obtained using Eqs. 27a–27d with boundary conditions (28a–28f). The zero-order temperature and von Mises stress are computed using Eqs. 14a–15 and (18). A typical set of parameters used in our computations is listed in Table 1. For all computations, we assume that the top of the crystal is insulated from the chuck ($\delta_0 = 0$) and the mean heat-transfer coefficient is $\bar{h}_{gs} = 4\,\mathrm{W/m^2K}$.

4.1 Combined convective and radiative heat transfers

We assume that a desirable crystal shape can be produced by adjusting the pulling rate; the non-dimensional heat flux of the melt is $\gamma = -0.1$. A negative γ means that the melt region near the crystal/melt interface is a supercooled region. This γ can be obtained through controlling the melt flow. The assumption of a constant heat flux from the melt is based on an observation of the manufacturing process for InSb using the Cz method [7]. It has been observed that the bottom of the crystals is almost flat (except at the triple point) and the power supply stays stable (indicating a steady heat flux).

Table 1 A summary of parameters for InSb growth

Name	Symbol	Value
Ambient gas temperature	T_g	600 K
Melting temperature	T_m	798.4 K
Solid density	ρ_s	5.64×10^3 kg/m^3
Liquid density	ρ_l	6.47×10^3 kg/m^3
Thermal conductivity	k_s	4.57 W/m K
Heat capacity	$\rho_s c_s$	1.5×10^6 J/m^3 K
Surface-tension coefficient	σ	0.434 J/m^2
Latent heat of fusion	L_h	2.3×10^5 J/kg
Mean crystal radius	$\bar{R}$	0.03 m
Crucible radius	R_c	0.1 m
Equilibrium growth angle	θ_c	25°

Before we present our main results, we will discuss briefly the case of cylindrical crystals in Sect. 4.1.1. The main purpose is to show that our procedure produces consistent results compared to the ones reported in the literature for silicon [4]. As noted earlier, it is extremely difficult to grow InSb crystals of cylindrical shape [7] and it has been shown in our previous paper [5] that stress levels are much higher in cylindrical crystals than that in conic ones. Therefore, we will focus our discussions on conic crystals in Sect. 4.1.2 before discussing shape optimization in Sect. 4.1.3.

4.1.1 Optimal β for cylindrical crystals

Although in this paper our main focus is on InSb crystals, our model is also applicable to other crystals. We start by applying our procedure to cylindrical silicon crystals so that a qualitative comparison can be made with the results obtained in [4]. Our computations are carried out by using the following parameter values. Density of the silicon crystal = 2420 kg/m^3; heat capacities = 1000 J/kg K; thermal conductivities $k_s = 22$ W/m K; Poisson's ratio = 0.25; crystal radius = 0.1 m; melting temperature = 1683 K; $T_g = 600$ K; surface-tension coefficient = 0.72 J/m^2; latent heat of fusion = 1.8×10^6 J/kg; specific heat $c_s = 1000$ J/kg K; mean heat-transfer coefficient $h_{gs} = 8$ W/m^3 K and length of crystal = 0.6 m.

Figure 3(a) shows the profiles for optimal and constant h_{gs}. The following parameters are used to find the optimal solution: $\rho = 60$; $\omega_1 = 0.2$; $\omega_2 = 0.3$; $\beta_0 = 1.0$. Figure 3(b) shows the nondimensional temperature along the lateral surface at the end of growth. The history of the non-dimensional maximum von Mises stress corresponding to the optimal and constant heat-transfer coefficient h_{gs} is shown in Fig. 3(c). Figure 3(d) shows the non-dimensional von Mises stress along the lateral surface at the end of growth.

The results show that the stress level can be reduced by almost 50%, when the heat-transfer coefficient profile is optimized. The results also show that for the optimal case, the lateral temperature variation is smaller near the crystal/melt interface, which is consistent with the solution in [4] when the surface temperature itself is used as a control variable in the optimization process.

For an InSb crystal we assume that the mean radius of the crystal is 0.03 m. Figure 4(a) shows the corresponding optimal heat-transfer coefficient. The following parameters are used to find the optimal solution: $\rho = 60$; $\omega_1 = 0.2$; $\omega_2 = 0.3$; $\beta_0 = 1.0$. Figure 4(b) shows the non-dimensional temperature along the lateral surface at the end of growth. The history of the maximum von Mises stress corresponding to the optimal and constant heat-transfer coefficient h_{gs} is given in Fig. 4(c). Figure 4(d) shows the von Mises stress along the lateral surface at the end of growth. From Fig. 4(c) it can be seen that the thermal stress can be greatly reduced, similar to the results for silicon crystals.

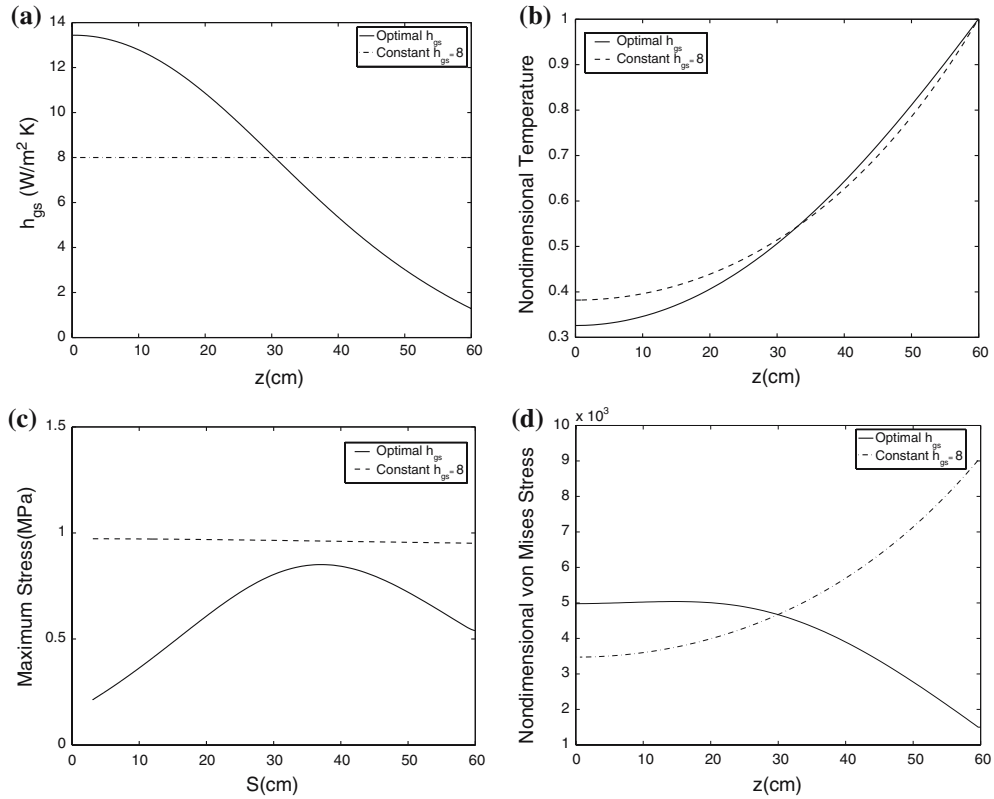

Fig. 3 **(a)** The optimal and constant heat-transfer coefficient h_{gs} for a silicon crystal. **(b)** The temperature along the lateral surface at the end of growth. **(c)** The history of non-dimensional maximum von Mises stress corresponding to the optimal and constant heat-transfer coefficient h_{gs}. **(d)** The non-dimensional von Mises stress along the lateral surface at the end of growth

4.1.2 Optimal β for conical crystals

The following results are for a conical crystal that is 33.5 cm long and 6 cm in diameter (largest), so that the mean radius is comparable to the cylindrical one of the previous section. We assume that $\beta_0 = 1$. To begin, we present some numerical results for three heat-transfer coefficients: constant, optimal, and experimental heat-transfer coefficient $h_{gs}(z)$. The experimental heat-transfer coefficient was estimated and communicated to us by the engineers we have been working with [7]. The optimal heat-transfer coefficient is calculated when $\omega_1 = 0$, $\omega_2 = 0.3$, and $\rho = 20$. In Fig. 5 we plotted the shape of β (or h_{gs}) used for comparison: constant, one fitted from experimental data and the optimal function (obtained by solving the Euler–Lagrange equations derived in the previous section).

In Fig. 6(a) the maximum von Mises stress during growth is plotted. The parameters for the optimization problem are $\rho = 20$, $\omega_1 = 0$ and $\omega_2 = 0.3$. The stress at the end of growth is plotted in Fig. 6(b). It can be seen that the reduction of the stress using the optimal h_{gs} is quite dramatic.

Next we investigate the effect of the parameters in the optimization setup on the solutions. For the penalty parameter ρ, we find that the optimization problem converges to same solution when $\rho \geq 20$ for given ω_1 and ω_2 values. Figure 7(a) shows two optimal solutions of h_{gs} for $\omega_2 = 0$ and $\omega_2 = 0.4$ when $\omega_1 = 0$ and $\rho = 20$. Figure 7(b) shows the maximum von Mises stress during growth for these two cases. We found that the von Mises stress with $\omega_2 = 0$ is slightly lower than that for the $\omega_2 = 0.4$ case. Since the penalty associated with ω_2 determines the growth speed, the gain on stress reduction is at the expense of a longer growth time. For example, the growth time for $\omega_2 = 0$ (33.47 h) is longer than that for $\omega_2 = 0.3$ (30.68 h).

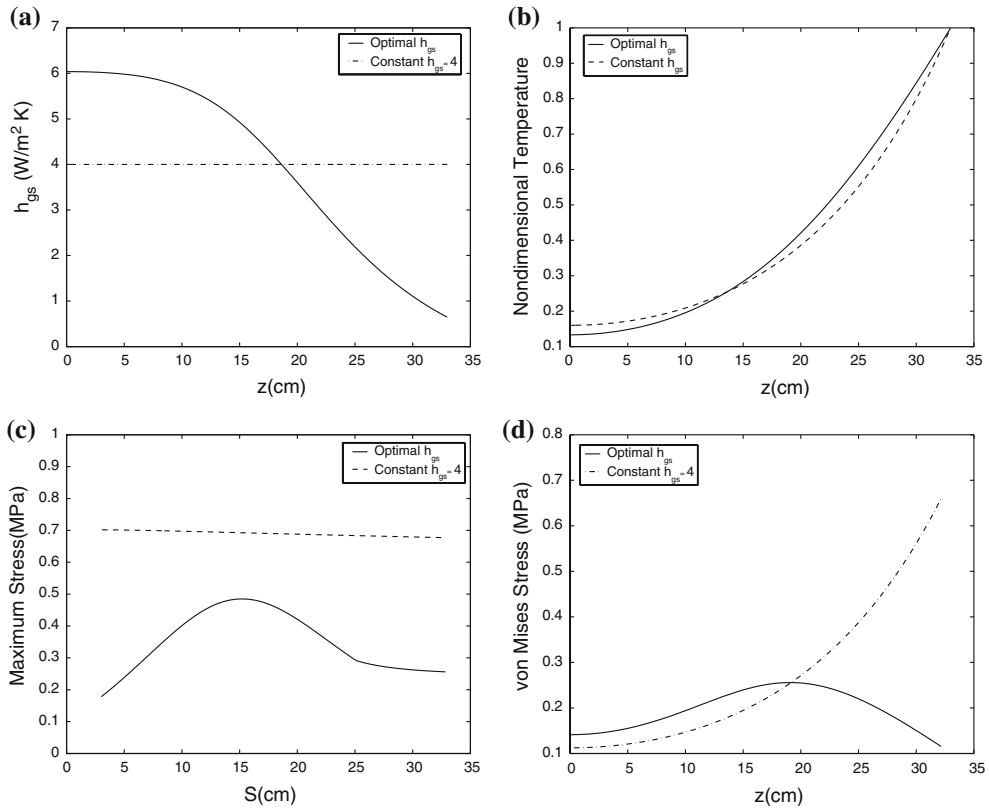

Fig. 4 **(a)** The optimal and constant heat-transfer coefficient h_{gs} for an InSb crystal. **(b)** The temperature along the lateral surface at the end of growth. **(c)** The history of maximum von Mises stress corresponding to the optimal and constant heat-transfer coefficient h_{gs}. **(d)** The von Mises stress along the lateral surface at the end of growth

Fig. 5 The three heat-transfer coefficients

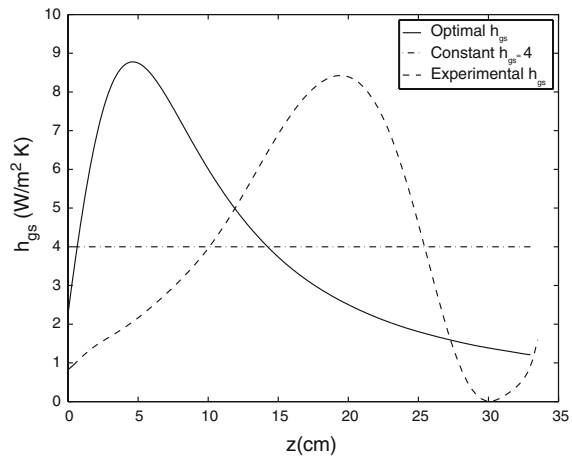

In order to investigate the robustness of the optimal solution, we present a set of calculations corresponding to a perturbation of the heat flux from the melt γ. We used the same optimal heat-transfer coefficient shown in Fig. 5 and computed the maximum von Mises stress $\sigma_{\max}$ corresponding to $\gamma = -0.1$, $\gamma = -0.09$

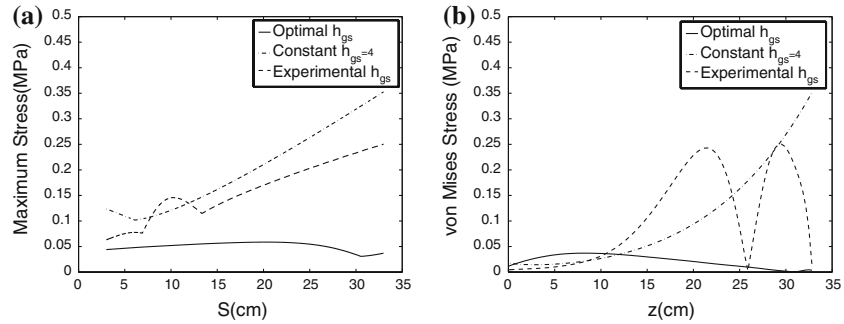

Fig. 6 **(a)** Maximum von Mises stress during the growth. **(b)** von Mises stress along the crystal lateral surface at the end of the growth. For the optimal heat-transfer coefficient the following parameters are used: $\rho = 20$, $\omega_1 = 0$ and $\omega_2 = 0.3$

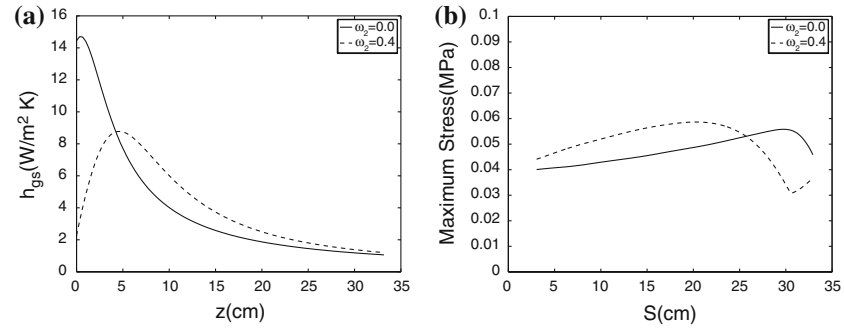

Fig. 7 **(a)** Optimal heat-transfer coefficients; **(b)** Maximum von Mises stress during growth for the parameters values $\omega_2 = 0$ and $\omega_2 = 0.4$, respectively. The other parameter values are $\omega_1 = 0$ and $\rho = 20$

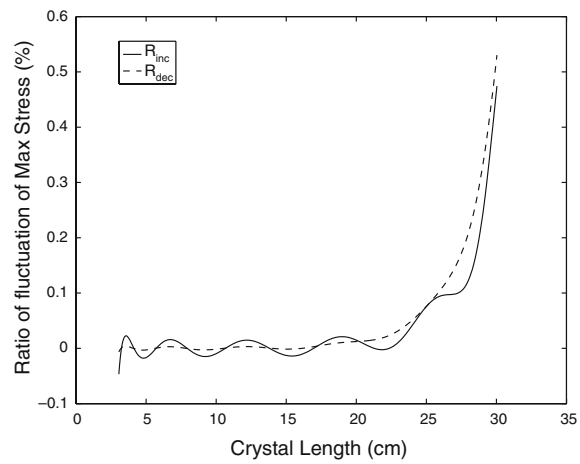

Fig. 8 The ratio of the fluctuation of the history of the maximum von Mises stress with an increase of 10% of the heat flux from −0.1 and a decrease of 10% of the heat flux from −0.1. The optimal shape used for the calculations is presented in Fig. 5

and $\gamma = -0.11$, denoted by $\sigma_{\max}^{-0.09}$, $\sigma_{\max}^{-0.1}$, $\sigma_{\max}^{-0.11}$, respectively. We define the ratio of the fluctuations as

$$R_{\text{dec}} = \frac{\sigma_{\max}^{-0.11} - \sigma_{\max}^{-0.1}}{\sigma_{\max}^{-0.1}}, \quad R_{\text{inc}} = \frac{\sigma_{\max}^{-0.09} - \sigma_{\max}^{-0.1}}{\sigma_{\max}^{-0.1}}.$$

From Fig. 8, it can be seen that the ratio of the fluctuation is less than 0.6% for a 10% deviation of the heat flux, which is small compared to the reduction of the stress by using the optimal h_{gs}.

Finally, we note that, while the optimization process works well in reducing the stress level, it is also evident that, in general, the stress level is much lower in a conic crystal than in a cylindrical one of similar

size, regardless of the optimization process. In the following we explore the possibility of further reducing thermal stress by shape optimization.

4.1.3 Optimal shape

The following calculations are for a crystal with a length of 33.5 cm and a seed crystal radius of $R_0 = 0.5$ cm. The mean crystal radius is $\bar{R} = 0.03$ m. We fix the slope of the crystal shape around $\tan 15°$. The parameters used for the optimization are $\rho = 20$, $\omega_1 = 0.1$, and $\omega_2 = 0.5$.

Figure 9(a) shows the linear h_{gs} used for the computation. Figure 9(b) is the optimal shape obtained by solving the Euler–Lagrange equations and a conical shape. Figure 9(c) shows the maximum von Mises stress corresponding to the optimal shape and the conical shape, respectively. Figure 9(d) shows the angle of the crystal shape in the (z, r) coordinate system corresponding to the optimal shape. We can see that the reduction in thermal stress is significant, while the slope of the crystal shape remains smooth with a slight increase of growth angle.

For the next set of computations we used an optimal h_{gs} obtained for a conical crystal. Figure 10(a) shows the shape of the optimal h_{gs}. Figure 10(b) shows the optimal shape obtained using $\rho = 20$, $\omega_1 = 0.1$, and $\omega_2 = 0.5$ with the conical shape. Figure 10(c) shows the maximum von Mises stress corresponding to the optimal shape and the conical shape, respectively. Figure 10(d) shows the angle of the optimal crystal shape in the (z, r) coordinate system. In this case, the reduction of the stress is not as significant, which shows that h_{gs} is nearly optimal, even though it is obtained with a given conical shape.

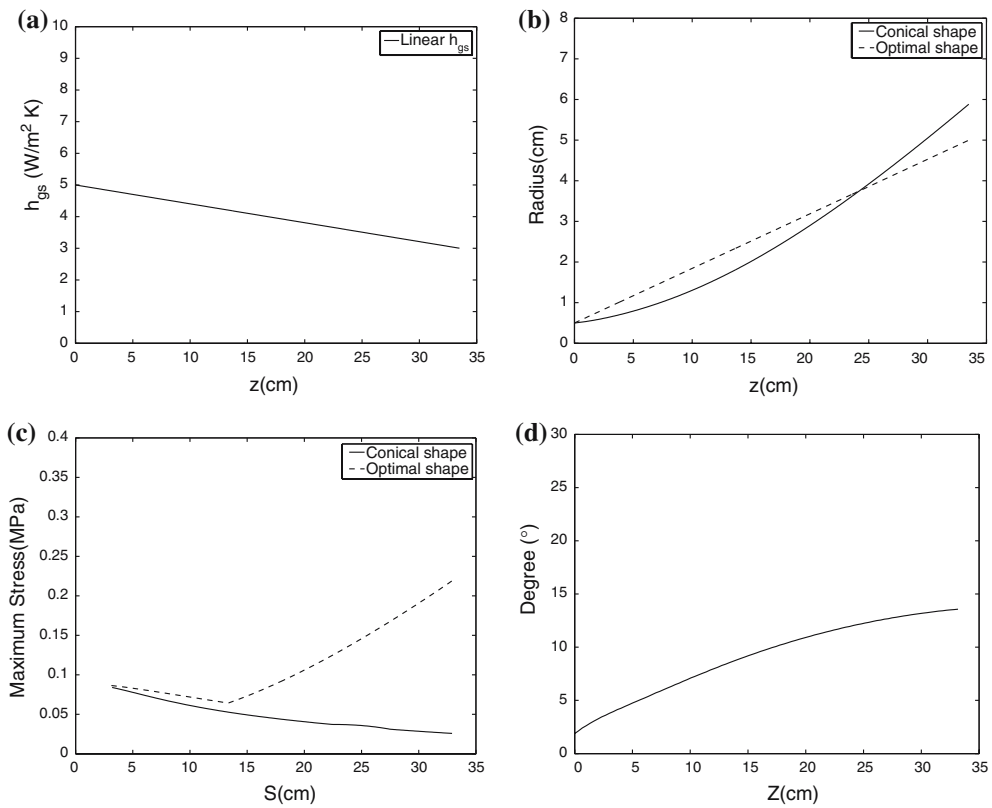

Fig. 9 **(a)** The given linear h_{gs}. **(b)** The optimal shape corresponding to the given h_{gs} when $\rho = 20$, $\omega_1 = 0.1$, and $\omega_2 = 0.5$ and a conical shape. **(c)** The history of the maximum von Mises stress corresponding to the optimal shape and the conical shape. **(d)** The degree of the crystal profile in the (z, r) coordinate system for the optimal shape

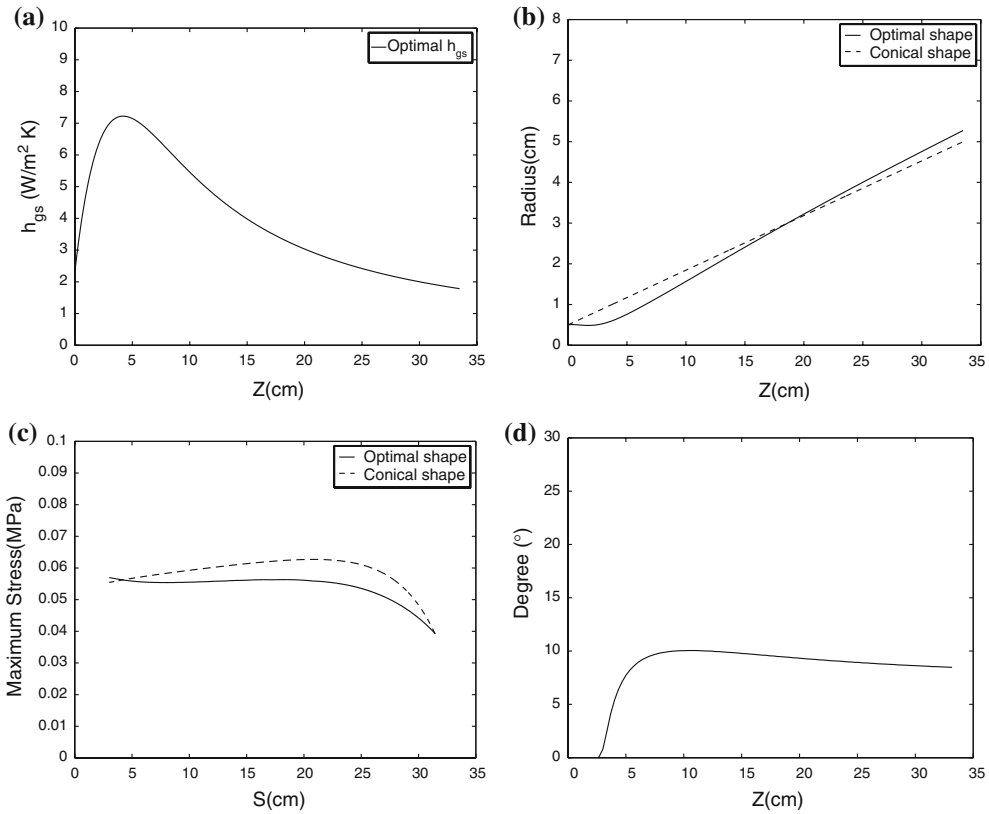

Fig. 10 **(a)** The given optimal h_{gs}. **(b)** The optimal shape corresponding to the given h_{gs} when $\rho = 20$, $\omega_1 = 0.1$, and $\omega_2 = 0.5$ and a conical shape. **(c)** The history of the maximum von Mises stress corresponding to the optimal shape and the conical shape. **(d)** The degree of the crystal profile in the (z, r) coordinate system for the optimal shape

We also carried our parameter studies and found that nearly the same solution is obtained for $\rho \geq 15$; $R_0' = \tan 15°/\sqrt{\epsilon}$ and $R_0' = \tan 6°/\sqrt{\epsilon}$. Figure 11 shows the effect of the parameter ω_1 on the optimal solution. The linear profile of h_{gs} is shown in Fig. 11(a). Figure 11(b) shows the optimal shape affected by parameter ω_1. Figure 11(c) shows the effect on the maximum von Mises stress. Figure 11(d) shows the angle of the crystal shape in the (z, r) coordinate system affected by ω_1. In general, the effect of ω_1 is small.

In order to study the robustness of our optimal solution, we use the optimal shape calculated using the given linear heat-transfer coefficient (Fig. 9) for the calculations. We assume the perturbation of the heat flux γ is 10% and use the same notation as in Sect. 4.1.2. Figure 12 shows that the fluctuation in stress is less than 0.07%.

Remark We have shown that significant stress reduction can be achieved by optimizing either the heat-transfer coefficient or the crystal shape. This is due to the fact that there are two contributing factors in the thermal stress, as shown in (18). By taking advantage of the inter-play of these two contributing factors, we can search for the best conditions for these two components to cancel out. To show this, we have plotted the components of the stress. Figure 13(a) shows the $R'\Theta_{0,z}$ component and the $\beta\Theta_0$ component of the von Mises stress σ_{VM} and the combination of the two components along the crystal profile at the end of growth of the crystal for the conical crystal shape. Figure 13(b) shows the $R'\Theta_{0,z}$ component and the $\beta\Theta_0$ component of the von Mises stress σ_{VM} and the combination of the two components along the crystal profile at the end of growth of the crystal for the optimal crystal shape. The heat-transfer coefficient used for the calculations is assumed to be linear.

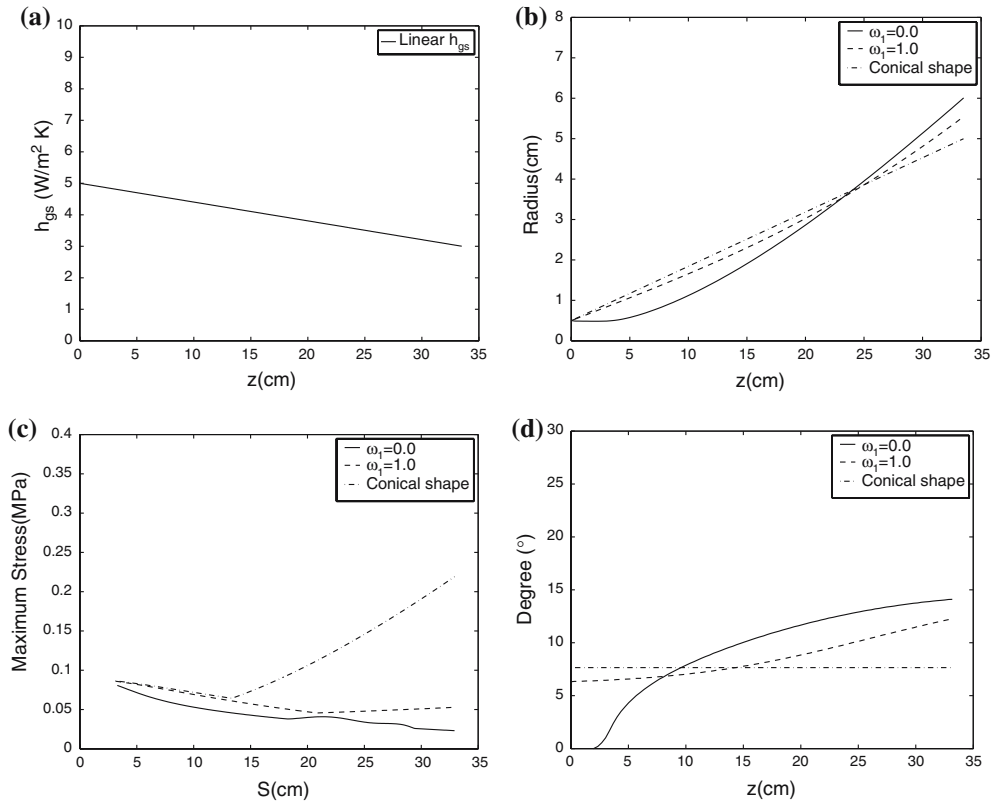

Fig. 11 **(a)** The given linear h_{gs}. **(b)** The two optimal crystal shapes for $\omega_1 = 0.0$ and $\omega_1 = 1.0$. **(c)** The history of the maximum von Mises stress during the growth of the crystal for $\omega_1 = 0.0$, $\omega_1 = 1.0$ hen $\rho = 20$, $R_0' = \tan 15°/\sqrt{\epsilon}$, and $\omega_2 = 0.1$ and conical shape. **(d)** The degree of the crystal profile in the (z, r) coordinate system for $\omega_1 = 0.0$ and $\omega_1 = 1.0$

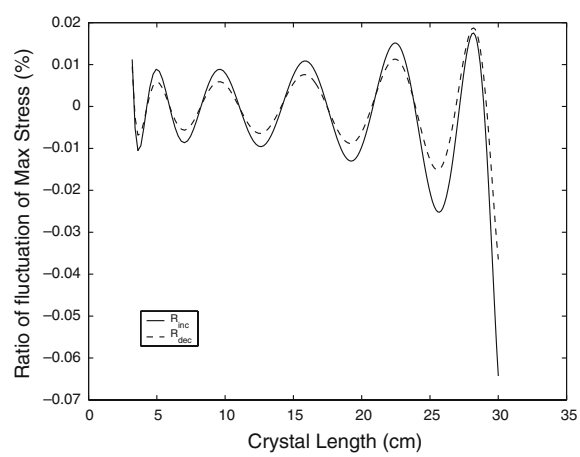

Fig. 12 The ratio of the fluctuation of the history of the maximum von Mises stress with an increase of 10% of the heat flux from −0.1 and a decrease of 10% of the heat flux from −0.1. The optimal shape used for the calculations is presented in Fig. 9

4.2 Effect of radiative transfer

We now treat the radiative heat transfer separately from the convective heat transfer. We assume that only the convective heat-transfer coefficient can be optimized. The numerical results presented in this section are obtained using the radiation model (2). We assume that a desirable crystal shape can be produced by

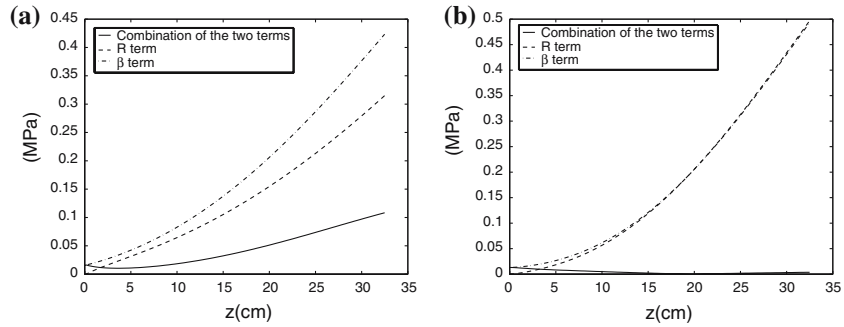

Fig. 13 **(a)** $R'\Theta_{0,z}$ component and $\beta\Theta_0$ component of the von Mises stress σ_{VM} and the combination of the two components along the crystal profile at the end of growth of the crystal for the conical crystal shape. **(b)** $R'\Theta_{0,z}$ component and $\beta\Theta_0$ component of the von Mises stress σ_{VM} and the combination of the two components along the crystal profile at the end of growth of the crystal for the optimal crystal shape when $R_0' = \tan 15^\circ/\sqrt{\epsilon}$, $\rho = 20$, $\omega_1 = 0.5$, and $\omega_2 = 0.2$

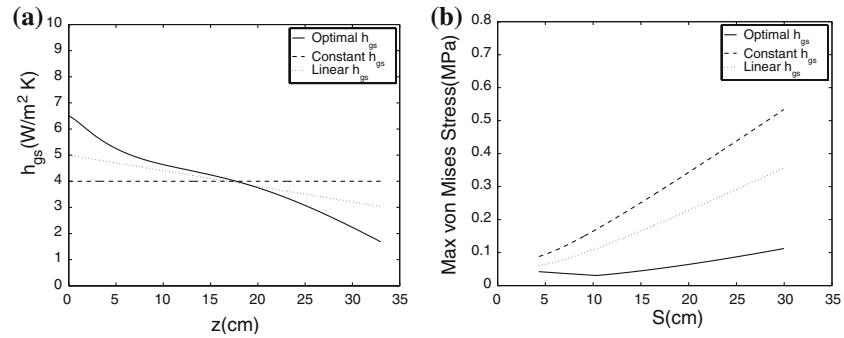

Fig. 14 **(a)** Three heat-transfer coefficients; **(b)** Maximum von Mises stress during the growth. For the optimal h_{gs} we used the following parameters: $\rho = 20$; $\omega_1 = 0.3$; $\omega_2 = 0.2$; $\beta_0 = 1.0$

adjusting the heat flux of the melt with a given pull rate of 2.2 cm/h and the radiative transfer coefficient is $r_c = 5.24 \times 10^{-9}\,\mathrm{W/(m^2\,K^2)}$.

4.2.1 Optimal β

For a given conical crystal shape we assume the radius of the seed crystal is $R_0 = 0.5$ cm, the length and the maximum radius of the crystal at the end of growth are 33.5 cm and $R_{\max} = 5.7$ cm, respectively. The following parameters are used for all optimization calculations: $\rho = 20$; $\omega_2 = 0.2$; $\beta_0 = 1.0$.

Figure 14(a) shows the shape of three heat-transfer coefficients. We used $\omega_1 = 0.3$ for the optimization problem. Figure 14(b) shows the maximum von Mises stress during the growth of the crystal for these three h_{gs}. Again, the reduction of the thermal stress using the optimal h_{gs} is significant.

We also performed parameter studies and found that different parameter values produce the same solution when ρ is greater than critical values. Robustness tests also yield similar results as before.

4.2.2 Optimal shape

We present the following optimal solutions for the given heat-transfer coefficients h_{gs}. For all the calculations we assume that the crystal length is 33.5 cm, the radius of the seed crystal is $R_0 = 0.005$ m, and the mean crystal radius is $\overline{R} = 0.03$ m. We assume the slope of the crystal profile is around $\tan 10^\circ$. The parameters used for the optimization are $\rho = 20$ and $\omega_2 = 0.6$.

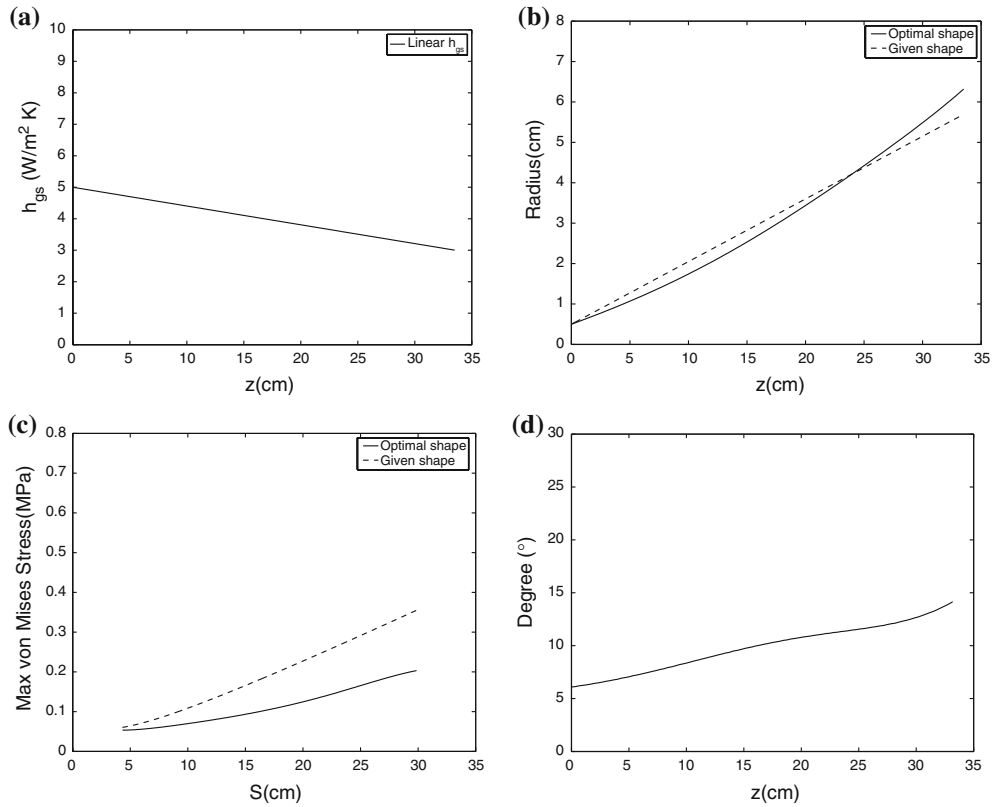

Fig. 15 **(a)** The given linear h_{gs}. **(b)** A given conical shape and the optimal shape. The parameters used for finding the optimal shape are as follows: $\omega_1 = 0.2$, $\omega_2 = 0.6$, $\rho = 20$, and $R_0' = \tan 10°/\sqrt{\epsilon}$. **(c)** The maximum von Mises stress for the two shapes. **(d)** The degree of the crystal profile in the (z, r) coordinate system for the optimal shape

Figure 15(a) shows the heat-transfer coefficient used for finding the optimal shape. Figure 15(b) shows a given conic shape and the optimal shape. The parameters used for finding the optimal shape are as follows: $\omega_1 = 0.2$, $\omega_2 = 0.6$, $\rho = 20$, and $R_0' = \tan 10°/\sqrt{\epsilon}$. Figure 15(c) compares the maximum von Mises stress and the stress at the final length for the two shapes. Reduction in thermal stress is again apparent when the optimal shape is used.

We have carried out a parameter study, a sensitivity analysis (robustness) and computed combined β and shape optimizations. The numerical results are similar to those obtained earlier for the combined convective–radiative heat-transfer case. It suggest that our optimization procedure is relatively robust. Even when part of the heat transfer (radiative) can not be optimized, the procedure we used seems to be able to find the suitable crystal shape which can reduce the stress significantly.

5 Conclusions

One of the main concerns of using the Czochralski technique to grow single compound crystals is the difficulty of controlling the appearance of crystalline defects. In practice, one has to find a suitable thermal environment and "magic shapes" (defined by the axial variation of the lateral surface) by trial-and-error so that defect-free crystals can be grown. The "shape effect" is not a serious issue for more commonly used single-material crystals such as silicon where cylindrical crystals are routinely grown. For compound crystals, however, it is extremely difficult to grow defect-free crystals of cylindrical shape due to their

low resistance to resolve stress. As a result, shape control become a critical issue in practice [6, 7]. The combination of shape and thermal effects on defect distribution is not easy to manipulate and the control process is more delicate.

The shape effect was demonstrated in [5] where an explicit formula for the von Mises stress was derived. The thermal-stress level is determined by heat flux through the lateral surface and the shape variation of the lateral surface. When the growth condition is not optimized, these two components both contribute to the overall stress. On the other hand, if the growth process is controlled carefully, it is possible to find optimal conditions so that these two components cancel out. However, finding the most favorable conditions to balance these two components is not trivial.

By setting up a constrained-optimization problem within the framework of optimal control, we are able to approach the stress-reduction problem systematically. An optimal-control methodology provides a valuable tool and has been used previous in the crystal-growth literature. However, most of the previous studies assumed a simple cylindrical geometry for the crystal which is appropriate for growing silicon and other common single crystals. In this paper, we have discussed both the thermal and shape effects. By using an semi-analytical solution for the thermal stress, the optimization process is more efficient than a full numerical simulation. We are able to show that stress can be reduced significantly by choosing a suitable thermal environment (lateral heat flux) or by growing the crystal into an optimal shape.

In order to keep our problem mathematically manageable, we have made several simplifications. As a consequence, direct application of our results may not be suitable for a complicated growth procedure. Verification of our model is necessary and work is currently underway to incorporate the effect of melt flow. Nevertheless, the results reported provide useful insights and can be used as a general guide, especially when the melt flow can be controlled using various techniques such as the electromagnetic field.

Acknowledgements We would like to thank Bill Micklethwaite, S. Bohun and I. Frigaard for valuable discussions during the course of the research which eventually leads to this manuscript. Financial support from NSERC, MITACS, Firebird and BC ASI are gratefully acknowledged. Thanks also go to Professor H.K. Kuiken and the anonymous referees for their constructive comments and suggestions.

Appendix A: Euler–Lagrange equations for optimization problem I

Using the calculus of variations, we derive the first-order necessary conditions for the optimization problem given by Eq. 23 with the constraints (19a–19e).

Taking the first variation of (23) and using product rule yields

$$
\begin{aligned}
\delta J_1 = {} & \delta \int_0^L \left[\left(R'(z)\Theta_{0,z}(z) - \beta(z)\Theta_0(z) - f(\Theta_0(z)) \right) R(z) \right]^2 \mathrm{d}z \\
& + \delta \int_0^L \lambda(z) \left[\Theta_{0,zz}(z) + \frac{2}{R(z)} \left(R'(z)\Theta_{0,z}(z) - \beta(z)\Theta_0(z) - f(\Theta_0(z)) \right) \right] \mathrm{d}z \\
& + \omega_1 \delta \int_0^L \left(\beta(z) - \beta_0 \right)^2 \mathrm{d}z - \omega_2 \delta \int_0^L \Theta_{0,z}^2(z) \mathrm{d}z + \delta \left[\mu \left(\beta_0 L - \int_0^L \beta(z) \mathrm{d}z \right) \right] \\
& + \frac{\rho}{2} \delta \int_0^L \beta^2(z) H(-\beta(z)) \mathrm{d}z \\
= {} & \int_0^L 2R^2(z) \left[R'(z)\Theta_{0,z}(z) - \beta(z)\Theta_0(z) - f(\Theta_0(z)) \right] \\
& \times \left[R'(z)\delta\Theta_{0,z}(z) - \beta(z)\delta\Theta_0(z) - \Theta_0(z)\delta\beta(z) - f'(\Theta_0(z))\delta\Theta_0(z) \right] \mathrm{d}z \\
& + \int_0^L \delta\lambda(z) \left[\Theta_{0,zz}(z) + \frac{2}{R(z)} \left(R'(z)\Theta_{0,z}(z) - \beta(z)\Theta_0(z) - f(\Theta_0(z)) \right) \right] \mathrm{d}z
\end{aligned}
$$

$$+\int_0^L \lambda(z)\left[\delta\Theta_{0,zz}(z)+\frac{2}{R(z)}\left(R'(z)\delta\Theta_{0,z}(z)-\delta\beta(z)\Theta_0(z)-\beta(z)\delta\Theta_0(z)-f'(\Theta_0(z))\delta\Theta_0(z)\right)\right]\mathrm{d}z$$
$$+2\omega_1\int_0^L(\beta(z)-\beta_0)\,\delta\beta(z)\mathrm{d}z-2\omega_2\int_0^L\Theta_{0,z}(z)\delta\Theta_{0,z}(z)\mathrm{d}z$$
$$+\delta\mu\left(\beta_0 L-\int_0^L\beta(z)\mathrm{d}z\right)-\mu\int_0^L\delta\beta(z)\mathrm{d}z+\rho\int_0^L\beta(z)\delta\beta(z)H(-\beta(z))\mathrm{d}z$$

Using integration by parts for the above expression and the boundary conditions for Θ_0, we obtain the following after simplifying:

$$\begin{aligned}\delta J_1=\int_0^L\Big[&\lambda_{zz}-\left(\frac{2R'\lambda}{R}\right)_z-2\lambda\beta/R-2\beta R^2\left(R'\Theta_{0,z}-\beta\Theta_0\right)\\&-2\left(R^2R'\left(R'\Theta_{0,z}-\beta\Theta_0\right)\right)_z-2R^2\left(R'\Theta_{0,z}-\beta\Theta_0-f(\Theta_0)\right)f'(\Theta_0)\\&+2R^2\beta f(\Theta_0)-2\left(2RR'^2f(\Theta_0)+R^2R''f(\Theta_0)+R^2R'f'(\Theta_0)\Theta_{0,z}\right)\\&-2\lambda f'(\Theta_0)/R+2\omega_2\Theta_{0,zz}\Big]\delta\Theta_0\mathrm{d}z\\&+\int_0^L\left[\Theta_{0,zz}+\frac{2}{R}\left(R'\Theta_{0,z}-\beta\Theta_0-f(\Theta_0)\right)\right]\delta\lambda(z)\mathrm{d}z\\&-\int_0^L\left[2R^2\left(R'\Theta_{0,z}-\beta\Theta_0\right)\Theta_0+2\lambda\Theta_0/R-2\omega_1(\beta-\beta_0)+\mu-\rho\beta H(-\beta)\right]\delta\beta\mathrm{d}z\\&+\delta\mu\left(\beta_0L-\int_0^L\beta(z)\mathrm{d}z\right)+\frac{2R'\lambda}{R}\delta\Theta_{0,z}(L)\\&+\left[\lambda_z-\left(\delta_0+\frac{2R'}{R}\right)\lambda-2R^2R'\left[\left(R'\delta_0-\beta\right)\Theta_0-R'\delta_0\Theta_{ch}\right]-2R^2R'f(\Theta_0)\right]\delta\Theta_0(0)\end{aligned}$$

Since $\Theta_0(z)$, $\beta(z)$, $\lambda(z)$ and μ are arbitrary, the optimality conditions are obtained by setting the coefficients of $\delta\Theta_0(z)$, $\delta\beta(z)$, $\delta\lambda(z)$ and $\delta\mu$ equal to zero. The resultant conditions stated are exactly the Euler–Lagrange equations and the boundary conditions given in (24d–25d).

Appendix B: Euler–Lagrange equations for optimization problem II

We derive the first-order necessary conditions for the optimization problem given by Eq. 26 with the constraints (22a–22f) using the calculus of variations.

Taking the first variation of (26) and using the product rule yields

$$\begin{aligned}\delta J_2=&\,\delta\int_0^L\left[\left(R'(z)\Theta_{0,z}(z)-\beta(z)\Theta_0(z)-f(\Theta_0(z))\right)R(z)\right]^2\mathrm{d}z\\&+\omega_1\delta\int_0^L\left(R'(z)-R'_0\right)^2\mathrm{d}z-\omega_2\delta\int_0^L\Theta_{0,z}^2(z)\mathrm{d}z\\&+\delta\int_0^L\lambda(z)\left[R(z)\Theta_{0,zz}(z)+2\left(R'(z)\Theta_{0,z}(z)-\beta(z)\Theta_0(z)-f(\Theta_0(z))\right)\right]\mathrm{d}z\\&+\delta\left[\mu\left(L-\int_0^L R^2(z)\mathrm{d}z\right)\right]+\frac{\rho}{2}\delta\int_0^L\left(R(z)-R_0\right)^2H(R_0-R(z))\mathrm{d}z\\=&\int_0^L2\left[\left(R'(z)\Theta_{0,z}(z)-\beta(z)\Theta_0(z)-f(\Theta_0(z))\right)R(z)\right]\end{aligned}$$

$$
\begin{aligned}
&\left[\left(R'(z)\Theta_{0,z}(z)-\beta(z)\Theta_0(z)-f(\Theta_0(z))\right)\delta R(z)\right.\\
&\left.+\left(\delta R'(z)\Theta_{0,z}(z)+R'(z)\delta\Theta_{0,z}(z)-\beta(z)\delta\Theta_0(z)\right)R(z)\right]\mathrm{d}z\\
&+2\omega_1\int_0^L\left(R'(z)-R'_0\right)\delta R'(z)\mathrm{d}z-\omega_2\int_0^L 2\Theta_{0,z}(z)\delta\Theta_{0,z}(z)\mathrm{d}z\\
&+\int_0^L\delta\lambda(z)\left[R(z)\Theta_{0,zz}(z)+2\left(R'(z)\Theta_{0,z}(z)-\beta(z)\Theta_0(z)-f(\Theta_0(z))\right)\right]\mathrm{d}z\\
&+\int_0^L\lambda(z)\left[\delta R(z)\Theta_{0,zz}(z)+R(z)\delta\Theta_{0,zz}(z)\right.\\
&\left.+2\left(\delta R'(z)\Theta_{0,z}(z)+R'(z)\delta\Theta_{0,z}(z)-\beta(z)\delta\Theta_0(z)-f'(\Theta_0(z))\delta\Theta_0(z)\right)\right]\mathrm{d}z\\
&+\delta\mu\left(L-\int_0^L R^2(z)\mathrm{d}z\right)-\mu\int_0^L 2R(z)\delta R(z)\mathrm{d}z\\
&+\rho\int_0^L\left(R(z)-R_0\right)H(R_0-R(z))\delta R(z)\mathrm{d}z
\end{aligned}
$$

Using integration by parts for the above expression and the boundary conditions for $\Theta_0(z)$ and $R(z)$, we obtain the following after simplifying:

$$
\begin{aligned}
\delta J_2=&\int_0^L\left[R\Theta_{0,zz}+2\left(R'\Theta_{0,z}-\beta\Theta_0-f(\Theta_0)\right)\right]\delta\lambda\mathrm{d}z\\
&+\int_0^L\left[2\beta^2R^2\Theta_0+2R\left(\beta R\Theta_0-2RR'\Theta_{0,z}\right)R''+2\beta'R^2R'\Theta_{0,z}+R\lambda''-\lambda R''-2\beta\lambda\right.\\
&+2R^2\beta\Theta_0f'(\Theta_0)+2R^2f(\Theta_0)f'(\Theta_0)+4RR'2f(\Theta_0)+2R^2R''f(\Theta_0)\\
&\left.+2R^2\beta f(\Theta_0)-2\lambda f'(\Theta_0)+2\omega_2\Theta_{0,zz}\right]\delta\Theta_0\mathrm{d}z\\
&+\int_0^L\left[6RR'^2\Theta_{0,z}^2-12\beta\Theta_0RR'\Theta_{0,z}+6\beta^2R\Theta_0^2-2R^2R''\Theta_{0,z}^2+2\beta'R^2\Theta_0\Theta_{0,z}-2\omega_1R''\right.\\
&+2\beta R^2\Theta_{0,z}^2-\lambda\Theta_{0,zz}-2\lambda'\Theta_{0,z}-2\mu R+\rho\left(R-R_0\right)H(R_0-R)\\
&\left.-4RR'\Theta_{0,z}f(\Theta_0)+6R^2f^2(\Theta_0)+8R\beta\Theta_0f(\Theta_0)+2R^2f'(\Theta_0)\Theta_{0,z}^2\right]\delta R\mathrm{d}z\\
&+\delta\mu\left(L-\int_0^L R^2(z)\mathrm{d}z\right)+\lambda R\delta\Theta_{0,z}(L)\\
&+\left\{\lambda'R-\lambda R'+2R^2R'\left[\beta\Theta_0-\delta_0R'\left(\Theta_0-\Theta_{ch}\right)\right]\right.\\
&\left.+2\omega\delta_0\left(\Theta_0-\Theta_{ch}\right)+2R^2R'f(\Theta_0)\right\}\delta\Theta_0(0)\\
&+\left[2R^2\left(R_z\Theta_{0,z}-\beta\right)\Theta_{0,z}+2\lambda\Theta_{0,z}+2\omega_1\left(R'-R'_0\right)-R^2f(\Theta_0)\Theta_{0,z}\right]\delta R(L)
\end{aligned}
$$

Since $\Theta_0(z)$, $R(z)$, $\lambda(z)$ and μ are arbitrary, the optimality conditions are obtained by setting the coefficients of $\delta\Theta_0(z)$, $\delta R(z)$, $\delta\lambda(z)$ and $\delta\mu$ equal to zero. The resultant conditions stated are exactly the Euler–Lagrange equations and the boundary conditions given in (27a–28f).

References

1. Bornside DE, Kinney TA, Brown RA (1991) Minimization of thermoelastic stress in Czochralski grown silicon: application of the integrated system model. J Cryst Growth 108:779–805
2. Jordan AS, Caruso R, von Neida AR (1980) A thermoelastic analysis of dislocation generation in pulled GaAs crystals. The Bell Syst Tech J 59(4):593–637

3. Müller G (2002) Experimental analysis and modeling of melt growth processes. J Cryst Growth 237–239:1628–1637
4. Jeong JH, Kang IS (2002) Optimization of the crystal surface temperature distribution in the single-crystal growth process by the Czochralski method. J Comput Phys 177:284–312
5. Bohun S, Frigaard I, Huang H, Liang S (2006) A semi-analytical thermal stress model for the Czochralski growth of type III-V compounds. SIAM J Appl Math 66(5):1533–1562
6. Micklethwaite WF, Johnson AJ (2001) InSb: materials and devices. In: Capper P, Elliot CT (ed) Infrared detectors and emitters: materials and devices, chapter 7. Kluwer Academic Publishers, 177–204
7. Micklethwaite WF (2003) Firebird Semiconductors Ltd., Private communications
8. Armaou A, Christofides PD (2001) Crystal temperature control in the Czochralski crystal growth process. AICHE J 47(1):79–106
9. Margulies M, Witomski P, Duffar T (2004) Optimization of the bridgman crystal growth process. J Cryst Growth 266:175–181
10. Metzger M, Backofen R (2000) Optimal temperature profiles for annealing of GaAs-crystal. J Cryst Growth 220:6–15
11. Kuiken HK (1979) The cooling of low-heat-resistance cylinders by radiation. J Engng Math 13:97–106
12. Kuiken HK, Roksnoer PJ (1979) Analysis of the temperature distribution in FZ silicon crystals. J Cryst Growth 47(1):29–42
13. Brattkus K, Davis SH (1988) Directional solidification with heat losses. J Cryst Growth 91(4):538–556
14. Young GW, Heminger JA (1997) Modeling the time-dependent growth of single-crystal fibers. J Cryst Growth 178(3): 410–421
15. Young GW, Heminger JA (2000) A mathematical model of the edge-defined film-fed growth proccess. J Engng Math 38:371–390
16. Tatarchenko VA (1993) Shaped crystal growth. Kluwer Academic Publishers
17. Ivanov NG, Korsakov AB, Smirnov EM, Khodosevitch KV, Kalaev VV, Makarov YuN, Dornberger E, Virbulis J, von Ammon W (2003) Analysis of magnetic field effect on 3D melt flow in CZ Si growth. J Cryst Growth 250:183–188
18. Hurle DTJ (1995) A mechanism for twin formation during Czochralski and encapsulated vertical bridgman growth of III-V compound semiconductors. J Cryst Growth 147:239–250
19. Liang S (2005) Thermal stress reduction inside InSb crystal grown by Czochralski method. Ph.D. Dissertation, York University
20. Hurle DTJ, Rudolph P (2004) A brief history of defect formation, segregation, faceting, and twinning in melt-grown semiconductors. J Cryst Growth 264:550–564